Dalton Transactions

Accepted Manuscript

This article can be cited before page numbers have been issued, to do this please use: S. R. Mathis (II), S. T. Golafale, J. Bacsa, C. W. Ingram, A. Steiner, F. P. Doty, E. Auden and K. Hattar, *Dalton Trans.*, 2016, DOI: 10.1039/C6DT03755K.

This is an Accepted Manuscript, which has been through the Royal Society of Chemistry peer review process and has been accepted for publication.

Accepted Manuscripts are published online shortly after acceptance, before technical editing, formatting and proof reading. Using this free service, authors can make their results available to the community, in citable form, before we publish the edited article. We will replace this Accepted Manuscript with the edited and formatted Advance Article as soon as it is available.

You can find more information about Accepted Manuscripts in the author guidelines.

Please note that technical editing may introduce minor changes to the text and/or graphics, which may alter content. The journal's standard Terms & Conditions and the ethical guidelines, outlined in our author and reviewer resource centre, still apply. In no event shall the Royal Society of Chemistry be held responsible for any errors or omissions in this Accepted Manuscript or any consequences arising from the use of any information it contains.

ROYAL SOCIETY OF CHEMISTRY

rsc.li/dalton

View Article Online
DOI: 10.1039/C6DT03755K

Mesoporous Stilbene-based Lanthanide Metal Organic Frameworks: Synthesis, Photoluminescence and Radioluminescence Characteristics

Stephan R. Mathis II[a], Saki T. Golafale[a], John Bacsa[b], Alexander Steiner[c], Conrad W. Ingram[a]*, F. Patrick Doty[d], Elizabeth Auden[e], and Khalid Hattar[e]

a Center for Functional Nanoscale Materials Department of Chemistry, Clark Atlanta University, Atlanta, GA 30314, USA

b. Department of Chemistry, Emory University, Atlanta, GA 30322, USA

c. Department of Chemistry, University of Liverpool, Liverpool L69 7ZD, UK

d Sandia National Laboratories, Livermore CA, 94550, USA

e. Sandia National Laboratories, Albuquerque, NM87185, USA

**Correspondence email: cingram@cau.edu*

Abstract

Ultra large pore isostructural metal organic frameworks (MOFs) which exhibit both photoluminescence and scintillation properties, were synthesized from *trans* - 4, 4'-stilbenedicarboxylic acid (H_2**L**) and trivalent lanthanide (Ln) metal salts under solvothermal conditions (Ln = Er^{3+} (**1**) and Tm^{3+} (**2**)). This new class of mesoporous materials is a non-interpenetrating network that features ultra-large diamond shaped pores of dimensions with approximate cross-sectional dimensions of 28 Å x 12 Å. The fully deprotonated ligand, **L**, is isolated and rigidified as it serves as the organic linker component of the MOF structure. Its low density unit cells possess asymmetric units with two crystallographically independent Ln^{3+} ions in seven coordinate arrangements. A distinct feature of the structure is the *bis*-bidentate carboxylate groups. They serve as a ligand that coordinates two Ln(III) ions while each **L** connects four Ln(III) ions yielding an exceptionally large diamond-shaped rectangular network. The structure exhibits ligand-based photoluminescence with increased lifetime compared to free stilbene molecules on exposure to UV radiation, and also exhibits strong scintillation characteristics, comprising of both prompt and delayed radioluminescence features, on exposed to ionizing radiation.

View Article Online
DOI: 10.1039/C6DT03755K

Introduction

Metal organic framework (MOF) materials have shown great promise for applications in many areas. Examples include ionizing radiation detection[1], chemical sensing, adsorption, ion exchange, gas storage, catalysis, optics, magnetism, molecular recognition and drug delivery.[2] Their assembly involves coordination between metal ions or metal ion clusters and bridging linkers (usually organic ligands) to produce 2-D and 3-D structures. Cavities, voids, pores and channels are present in many cases. The three dimensional lattices of MOF structures offer well defined environments for the isolation of organic chromophores and consequently, luminescent MOFs that display ligand-based emission have been receiving increasing attention in recent years. Of particular interest is the potential application of MOFs as radioluminescent (scintillating) materials for the detection of ionization radiation, including neutrons, protons and gamma rays. Advancements in the science of ionizing radiation detection are of great interest and significance in radiography, biological safety, and nuclear materials identification and monitoring. The organic molecule, stilbene, is a very important radioluminescent component of many solid-state scintillating materials.[3] However, when exposed to ionizing radiation, stilbene can undergo *trans-cis* isomerization, and the non-fluorescent *cis* isomer can also produce additional photobyproducts, including cyclization to dihydrophenanthrene.[4,5] These events lead to energy loss through non-radiative relaxation that can significantly reduce luminescence efficiency and quantum yield.

Recently it was shown that incorporating *trans*-4,4'-stilbenedicarboxylate as the linker, **L**, in a Zn based MOF structure, suppresses its *trans-cis* isomerization activity, thereby producing a photoluminescent[6,7] and radioluminescent[1a,b] material with increased quantum efficiency. The ligand, **L** is a relatively long and flexible and when used in MOFs synthesis, the openness of any 3-D structures that are produced may be compromised by interpenetration of multiple nets, as was observed in Zn-stilbene MOFs reported.[6,8] Though the multiple nets can, in many cases, stabilize the structure by through-space inter-chromophore interactions between the neighbouring ligands, the interpenetration can also alter their luminescence behaviour and reduce their porosity. MOFs utilizing **L** as linker have also been described for Cd,[9-14] Co[15-17] Cu[18] Mn,[19] Ni[5,11] Pb[20,21] Zn[22,26] and recently, Zr[27]. To date however, reports of lanthanide-stilbene MOFs are scarce[28,29] and those with non-interpenetrating open 3-D structures are unknown. MOFs with open network structures are attractive since their channels

View Article Online
DOI: 10.1039/C6DT03755K

and pores are desirable in a wide range of applications, including molecular separations and catalysis. In this research, we seek to explore the synthesis of lanthanide based MOFs for applications as photoluminescent and radioluminescent materials. The rationale for the use of lanthanide ions is based on their large size and their high propensity for high coordination numbers, which can promote 3-D connectivity.

We report herein a new MOF structure that is prepared by reacting Ln(III) ions with H_2**L** (Ln = Tm (**1**) and Er (**2**)), and its associated photo- and radioluminescence properties. The non-interpenetrating, low density structure possesses ultra large pores with approximate cross-sectional dimensions of 28 Å x 12 Å. The framework isolates and imposes structural rigidity on the the **L** units by locking its ethylene group in a *trans* configuration. This serves to simultaneously reduce *trans-cis* isomerization and the degree of inter-chromophore interactions between the stilbene units. Non-radiative relaxation pathways are restricted as a result, thus enhancing its radiative photoluminescent and radioluminescence lifetimes.

Experimental

Materials and supplies

Trans-4,4'-stilbenedicarboxylic acid, H_2**L,** was purchased from Sigma Aldrich, Inc. Thulium nitrate ($Tm(NO_3)_3 \cdot 6H_2O$) was purchased from Alfa Aesar and erbium nitrate ($Er(NO_3)_3 \cdot 6H_2O$) was purchased from Acros Organics. N,N - diethylformamide (DEF) was purchased from TCI America. All chemicals were research grade and were used without further purification.

Synthesis

Structure **1** ($C_{64}H_{40}Er_3O_{21}$): A mixture of $Er(NO_3)_3 \cdot 6H_2O$ (75.4 mg, 0.17 mmol), H_2**L** (7.5 mg, 0.028 mmol) and DEF (5 mL) were sealed in an 8 mL scintillation vial and heated to 105°C for 48 h. The vial was allowed to cool and the colorless crystals were filtered and repeatedly washed with fresh DEF. The yield was 96 % based on H_2**L**. Elemental anal. Calcd (%): C, 46.7; H, 2.43. Found: C, 46.2; H, 2.86. FTIR (KBr pellet, cm^{-1}): 3478 br, 3144 br, 2981w, 2930w, 2855w, 1684w, 1544w, 1420s, 1101w, 958w, 785m, 707w, 630w, 574w, 526w.

View Article Online
DOI: 10.1039/C6DT03755K

Structure **2** ($C_{64}H_{40}Tm_3O_{21}$)**:** The procedure for the synthesis of **2** was similar to **1**, except $Tm(NO_3)_3 \cdot 6H_2O$ was used and the synthesis time was 20 h. The yield was 77 % based on H_2**L**. Elemental anal. Calcd (%): C, 46.5; H, 2.42; Found: C, 46.2; H, 2.66; FTIR (KBr pellet, cm^{-1}): 3478 br, 3144 br, 2981w, 2930w, 2855w, 1684w, 1544w, 1420s, 1101w, 958w, 785m, 707w, 630w, 574w, 526w.

Characterization

*Single crystal analysis***:** X-ray diffraction data (MoK_α) were collected on a Bruker APEX-II CCD diffractometer at 100 K. The diffraction intensities, even from very large crystals, were very weak due to its porous and low density structure which contains highly disordered solvent molecules in the voids. We speculate that the crystals may have been extensively twinned and this contributed towards the very weak diffraction. However, there were no obvious signs of twinning in the diffraction patterns. Complete intensity data were collected with the program, APEXII (Bruker). Cell parameters were refined using SAINT.[30] Data reduction, scaling and absorption corrections were performed using SAINT and SADABS-2014/5[31]. The structures were solved by charge flipping using the Superflip structure solution program[32] and by using Olex2[33] as the graphical interface.

A survey of the diffraction indicates weak and diffuse reflections commensurate with the defects in the crystal (a consequence of the strain in the structure). The systematic absences and the cell symmetry were consistent with the space group *Cmcm*. The refinements in *Cmcm* showed severe disorder. The non-isomorphic subgroups $Cmc2_1$, *C*2*cm* (*Ama*2) and *C*2/*c*, which all retain *C*-centered cell and *c*-glide plane were tested but also showed various types of disorder (see SI for details). A non-disordered model was finally obtained in space group *Cc*, which is a subgroup of the latter three that preserves both the lattice centering and the glide plane, in the form of a pseudo-merohedral twin. Platon Squeeze[34] was used to treat the disordered solvent and the contents of the voids because the electron density was too diffuse to model. The models were refined with ShelXL using Least Squares minimization.[35] All non-hydrogen atoms were refined anisotropically. Hydrogen positions were calculated geometrically and refined using the riding model.

View Article Online
DOI: 10.1039/C6DT03755K

Powdered X-ray diffraction (PXRD analysis was conducted using a Panalytical Empyrean Series II X-ray Diffractometer. The X-ray source was a Cu Kα (λ=1.5418 Å) anode operating at 45 kV and current of 40 mA, and diffraction patterns were obtained between the 2θ angles of 4˚- 40˚, with a step size of 0.026˚ and scan time of 147.5 seconds. Simulated PXRD patterns were obtained from SCXA data using Mercury 3.1 software from the Cambridge Crystal Data Center (CCDC).

Infrared measurements were recorded on a Bruker Alpha-P FT IR spectrophotometer (intensive pattern: m-medium, s-strong, w-weak). The sample was introduced into the spectrophotometer using KBr as a zero background powder and measurements were acquired between 350 cm^{-1} and 4000 cm^{-1}. Thermogravimetric analysis was conducted on a TA Instrument Q50 thermal analyzer. Approximately 2 mg of (chloroform soaked) **1** and **2** were heated at a rate of 5 °C/min from ambient temperature to 900°C under air flow. Elemental analysis was performed by Atlantic Microlab, Atlanta, GA, USA.

Room temperature solid-state photoluminescence measurements were carried out on a thin layer of crystals that was placed between quartz plates on a SPEX FluoroLog 3 spectrofluorimeter in its front face emission scan mode. Radioluminescence measurements were conducted using ion beam induced luminescence (IBIL) method in the Ion Beam Laboratory, Sandia Laboratories, New Mexico, using published proceduress.[1b] The experimental setup and conditions involved a 2.5 MeV proton beam, a current density 12000 NA/cm^2 with the sample under 4.3 x 10^{-6} Torr vacuum pressure and ambient temperature. The beam was focused onto the sample with a spot sized estimated to be 120 μm x 175 μm. Data was collected using a fiber optics coupled CCD spectrophotometer.

Time correlated single photon counting (TCSPC) was used to determine radioluminenscence decay dynamics. The instrument setup and operation were previously described.[1c] The setup includes a ^{137}Cs γ radiation source (0.66 MeV, 70.1 μCi), two photomultiplier tubes and a light tight box. The first PMT (Hamamatsu, H5783-04) is coupled to the sample to detect the trigger. The second PMT (Hamamatsu H9305-03) is equipped with an attenuator to reduce the amount of photons it received and processed by a digital oscilloscope (Lecroy Waverunner 6200A, 2 GHz). The sample was suspended between two glass coverslips with Visilox-788 optical grease, and mounted on the PMT lens. The ^{137}Cs source was placed

View Article Online
DOI: 10.1039/C6DT03755K

within close proximity of the sample, but not in the way of the PMTs so as to not interfere with data collection.

Results and Discussion

Structure Description

The X-ray crystal structures of $C_{64}H_{40}Er_3O_{21}$(**1**), and $C_{64}H_{40}Tm_3O_{21}$(**2**) show that both are isostructural and are open, 3-D non-interpenetrating frameworks with large pores (electronic supplemental information, ESI Figure S1 and Tables S1-S15). Details of the structure are therefore described herein for **1**. While the structures could be solved and refined in the higher symmetry of space group *Cmcm* (albeit with severe disorder), it was necessary to reduce the symmetry down to *Cc* in order to describe the detailed ordered framework that consists of metal ions and **L** linkers. The principle connectivity of the framework was determined, but the finer details of the structure are obscured by the twinning and disorder. In particular, there are strong Fourier artifacts along planes with Miller indices (100) that intersect the lanthanide atoms. The residual electron density along these planes obscure the coordination geometry about the lanthanide atoms. Interestingly, the stilbene ligands are not coplanar with these planes and refine relatively well.

A projection of the crystal structure on the *ab*-plane is shown in Figure 1. The low crystallographic symmetry of space group *Cc* generates an asymmetric unit containing four stilbene ligands and three metal ions (Er1, Er2 and Er3) two of which (Er2 and Er3) are symmetrically equivalent in the higher symmetry but diverge in their y-positions in the lower symmetry. The breaking of the symmetry from *Cmcm* to *Cc* may be the result of mechanical stress within the framework. The stilbene atoms are located easily but the coordinated DEF molecules are not. An interesting aspect of this structure is that the rigid ligand retains a nearly planar conformation and separates the Ln(III) corners by a distance of 17 Å. The stilbene linkers are not strictly planar but slightly bent, which may indicate strain within the framework.

All metal ions are seven-coordinated; Er2 and Er3 contain one extra ligand atom in their coordination sphere in addition to the six oxygen atoms which are part of carboxylate groups, while Er1 binds to three additional ligand atoms. The nature of these ligands is not clear from the refinements because the coordinated ligand atoms show large thermal parameters and the electron density surrounding these sites is very diffuse. One can assume that these sites are

View Article Online
DOI: 10.1039/C6DT03755K

partially occupied by disordered DEF solvent and/or water molecules. The metal ions are bridged by carboxylate groups of the ligand, forming undulating chains along the crystallographic *c*-axis (Figure 2). The repeat unit of the coordination chains contains three metal ions and eight carboxylate groups. Metal ions, Er2 and Er3, are bridged by four carboxylates while metal ion Er1 is joined to each of the other by two carboxylates (Figure 2). The chains are crosslinked *via* stilbene linkers resulting in a 3-D network.

The Er(III) atoms are the vertices linking the edges of the bridging ligands. The carboxylate ions are *bis*-bidentate and bridge two Er atoms rather than each carboxylate chelating one Er atom. It is interesting to reflect on the differences in these two modes of binding on complexing Ln^{3+} ions. Lanthanide atoms are very large and the longer O···O distances in neighbouring *bis*-bidentate carboxylate ions (2.5 Å – 3 Å) are better suited for forming optimal coordination geometries about the Ln^{3+} ions (with minimal strain) than the shorter O···O distance (2.2 Å) in the non-bridging carboxylate ion. On the other hand, the C=O···M angles are much wider (about 145°) when the carboxylate bridges two metals than when the carboxylate chelates one metal (nearly 90°). From an electron density perspective, there are two valence charge concentrations about the oxygen atom (corresponding to its lone pair electrons) approximately 115° to the C=O bond. It seems that chelating carboxylates are better at directing the lone pair maxima towards the metal atoms whereas bridging carboxylates optimizes the coordination geometry about the lanthanide atoms because of the flexible O···O distances. The bridging carboxylates form an infinite, undulating chain of Ln(III) atoms along the *c*-axis (Figure 2). The chain direction is perpendicular to the μ_4-ligand bridges. There are two groups of bridging carboxylate ligands (Figures 1a and 1b) perpendicular to the metal chains forming lattice planes with Miller indices of (1-10) and (-1-10) and a dihedral angle of 55° forming a complex infinite 3-D mesoporous network. These intersecting planes form a large molecular rectangle with a diagonal distances of 30.6 Å and 16.1 Å.

The molecular rectangles are aligned so that they form exceptionally large diamond shaped channels along the crystallographic direction [001] (Figure 3). The pore dimensions were estimated with the aid of the computer program, SECTION.[36] This program displays cross-sectional slices through the unit-cell (using van der Waals radii) and from which the size of the pores were measured. The channels are continuous and are about 28 Å x 12 Å wide when the additional ligand atoms that complete the coordination spheres of Er1 are included in the

View Article Online
DOI: 10.1039/C6DT03755K

measurement. They are intersected by smaller channels. A more precise estimate of the solvent accessible volume was determined using Platon[40] and amounts to 7850 Å^3 or 62% of the unit cell volume. The estimated surface area in the unit cell is 3353 Å^2. The channels are linear with not much variation in their widths. The pore region is likely to contain highly disordered solvent molecules. The electron density in this region is very diffuse and contributes little to the Bragg scattering. When viewed along the *b*-axis it becomes apparent that the architecture is supported by the diagonal bracing of stilbene linkers between the coordination chains, which reinforces the rigidity of the open framework (ESI Figure S4).

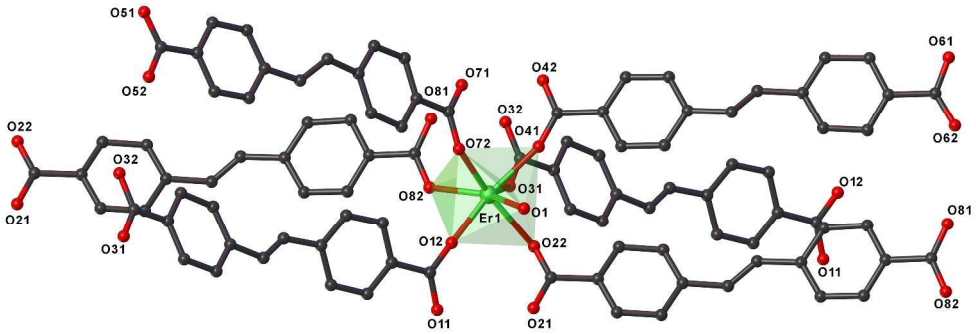

1a

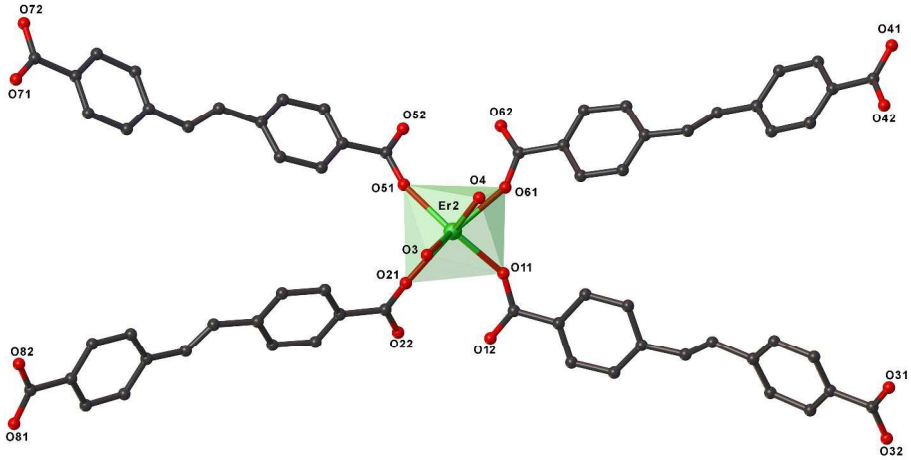

1b

Figure 1. Coordination environment of (a) Er1 and (b) Er2 in **1**. (Hydrogen atoms omitted for clarity).

View Article Online
DOI: 10.1039/C6DT03755K

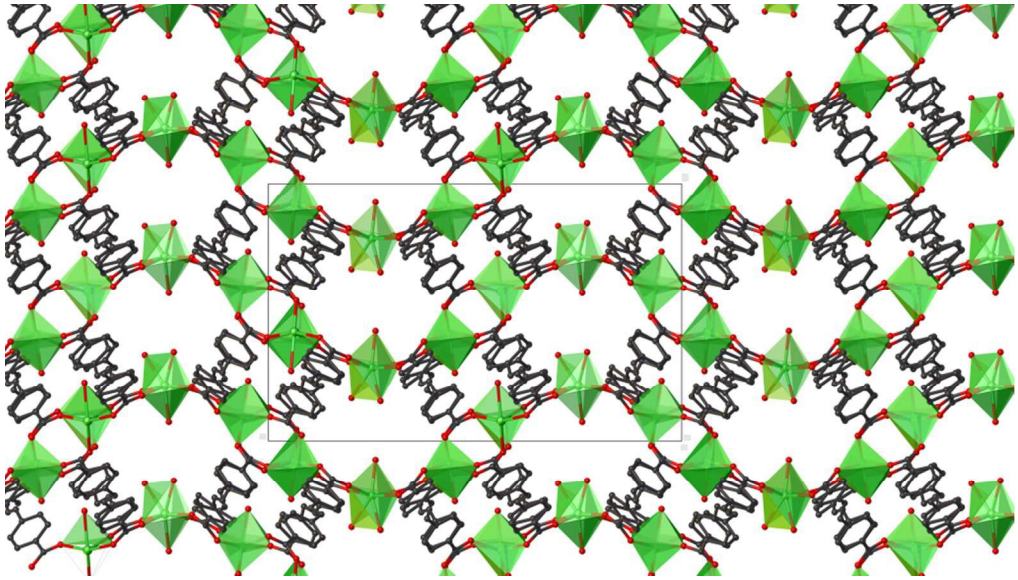

Figure 2. ErO_7 polyhedra (green) interconnected by ligand carboxylate groups, forming an undulating chain-like arrangement along the *c*-axis**,** and the interconnectivity of the undulating chains by **L** units along the (1-10) and (-1-10) directions in **1**. Hydrogen atoms and solvent molecules are omitted for clarity.

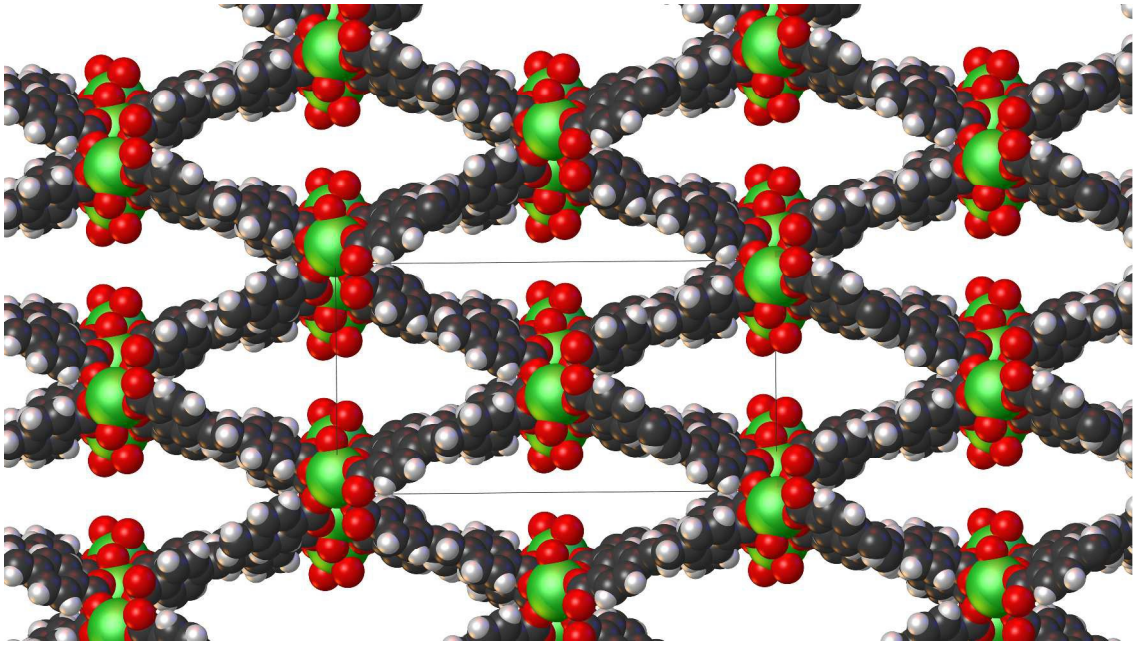

Figure 3. The structure from viewed along the [001] (channel) axis showing network of diamond-like channels. The atoms are drawn with 100% van der Waals radii. The inside diameters of the channels are about 28 Å x 12 Å. Solvent molecules are omitted for clarity.

View Article Online
DOI: 10.1039/C6DT03755K

Strikingly, this very low density mesoporous structure is devoid of interpenetrating networks. This is markedly different from the 2-D and 3-D MOF structures reported for this ligand with transition.[5,6,21] Structures **1** and **2** are also markedly different in their 3-D structural arrangement, space group, chemical composition, ligand-metal coordination and pore architecture from other reported stilbene-based lanthanide MOFs. Deng et al reported a series of stilbene-based lanthanide MOFs (Er included) which were synthesized from Ln_2O_3 (instead of the typical salt), HCl, and DMF at 180° C.[28] The structures crystallized as four different twofold interpenetrating 3-D pilllared layered networks, with formate ion (from the decomposition of DMF) and **L** units bridging the lanthanide ions. Song et. al reported that stilbene based Eu and Tb MOFs, which were synthesized at room temperature for 14 days, crystallized as twofold interpenetrating networks, and with the solvent, DMSO, coordinated to the framework structure.[29] The structures from these two lanthanide ion exists in different space groups and, are not similar those reported herein. Interestingly, the lanthanide ions are eight and nine coordinate in these reported MOFs, whereas they are seven coordinate in structures **1** and **2**. Further, the ligand exhibit three coordination modes (namely, chelating, bridging, and chelating-bridging) in the reported structures, whereas only the bridging coordination mode is present in structures **1** and **2**. The factors responsible for the open non-interpenetrating networks of structures **1** and **2** remain unclear, but the lower coordination number of the lanthanide ions and the coordination mode of the ligand are of interest.

Powder X-ray diffraction (PXRD) patterns of air dried structures, **1** and **2,** indicate that their diffraction profiles are both similar to their respective simulated pattern, as represented by that for **2** (ESI Figure S5). This further supports single crystal X-ray analysis, thus confirming that the compounds are isostructural. In addition, the close matching of diffraction peaks to the simulated pattern and the absence of additional peaks indicate that the structures crystallized as a pure phase.

FTIR spectra: FTIR spectral analysis shows that the peak around 1700 cm^{-1} in the H_2L disappears in the MOF structure due to the formation of -(CO_2)Er, thus indicating that the ligand is fully deprotonated within the structure (ESI Figure S6). The υ_{as}(C=O) absorption bands for the ligand at 1730 cm^{-1} and 1659 cm^{-1} redshift to 1629 cm^{-1} in **1** due to the formation of partial bond between oxygen atom and the Er atom which reduces the bond strength of C=O. In addition, **1** exhibits υ_s(C=O) absorption at 1406 cm^{-1} and 1328 cm^{-1}. The C-O stretching

View Article Online
DOI: 10.1039/C6DT03755K

vibrations are observed at 1140 and 1174 cm^{-1} in the pure ligand and at 1160 cm^{-1} in **1**. The IR spectrum of **2** shows similar features (ESI Figure S6).

Thermal analysis: For **1,** the TGA curve indicate weight loss of approximately 25 wt. % up to about 350 °C which is attributed to loss of DEF molecules from within the pores (ESI Figure S7). Further weight loss amounting to 25% between 520 °C and 600° is attributed to the degradation of the linker, with the metal oxide remaining as the solid residue. The TGA curve of **2** shows similar weight loss features. The structures are stable in air and in chloroform. However extended evacuation at ambient or elevated temparatures or exposure to solvents including water, methanol and methylene chloride in an effort to remove occluded DEF molecules, resulted in substantial irreversible structural changes with partial loss of crystallinity (as deterimined by powdered XRD). Consequently, the resulting material showed no significant surface area (as was determined by nitrogen porosimetry measurements) despite the porous crystal structure.

Photoluminescence

The isolation and rigidification of luminescent ligands by scaffolding them within MOF structures can significantly alter their properties from those exhibited when they are in their solid powdered form.[1] This luminescence behavior was investigated for **2** whose photoluminescence spectra are shown in Figures 4. The spectra of solid H_2L are also included for comparison.

View Article Online
DOI: 10.1039/C6DT03755K

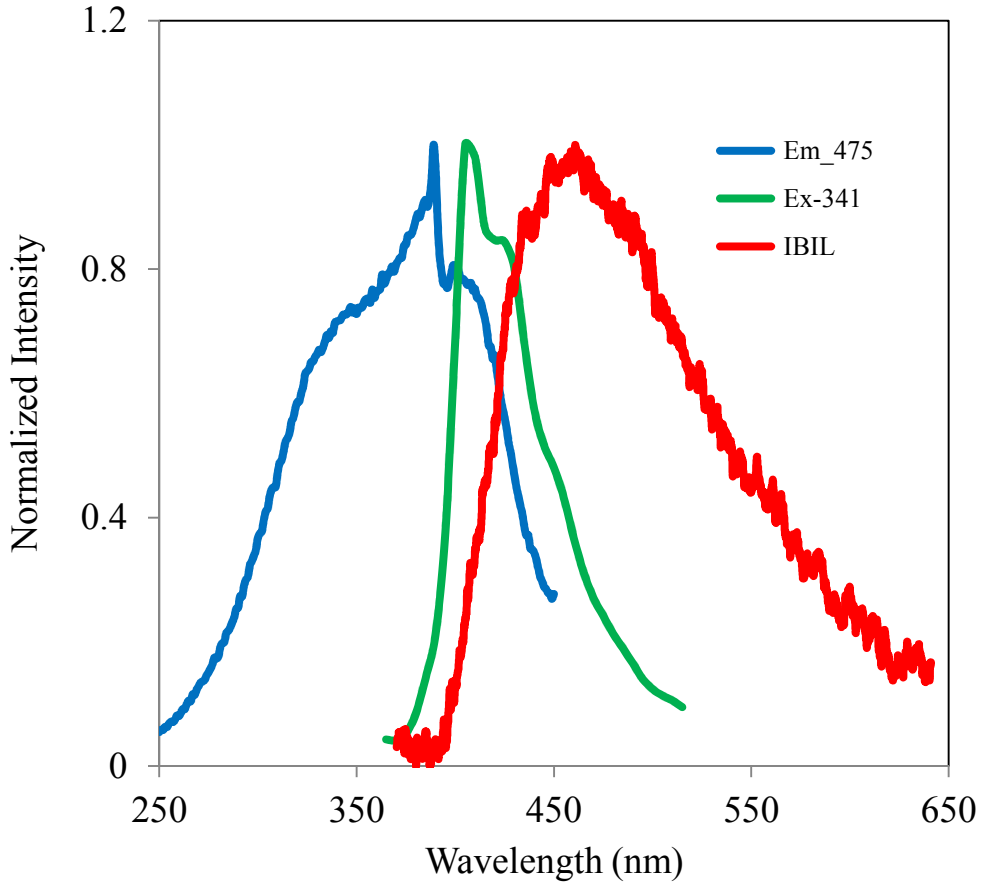

4a

View Article Online
DOI: 10.1039/C6DT03755K

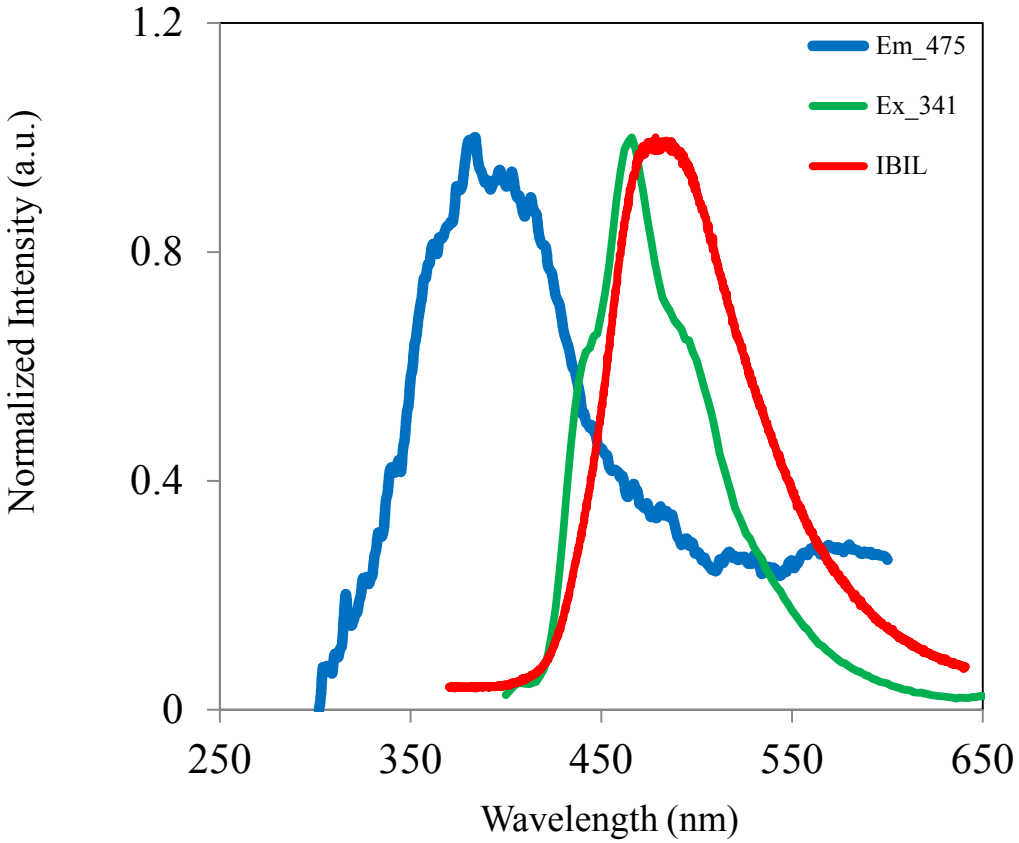

4b

Figure 4. Normalized excitation and photoluminescence spectra along with the ion bean induced luminescence (IBIL) spectra after exposure to 2.5 MeV proton beam of ionizing radiation for **2 (a)** and H_2**L**-powder (**b**).

The photoluminescence spectrum of structure **2** (Figure 4a) shows a profile, (consisting of distinct vibronic peaks), that is similar to that of H_2**L** (Figure 4b) and Na_2**L** in solution (ESI Figure S8) observed herein and reported elsewhere[37,38]. The profile is also similar to those reported for stilbenoid moieties in other structures[39], thus suggesting that the photoemission from **2** is linker based. Structure **2** exhibits Stokes shift of ~ 40 nm, which is smaller than the ~ 80 nm exhibited by H_2**L** powder. The Stokes shift is attributed to non-radiative relaxation pathway(s) in the structures upon UV excitation. A significant contributing factor to the non-radiative relaxation pathways is the electronic interactions among ligand units. In various reported structures containing the multiple units of **L** that are arranged in close proximity,

View Article Online
DOI: 10.1039/C6DT03755K

face-to-face (co-facial) electronic interactions between the units are known to depend on separation distances and angles between the aromatic ring planes, and the offset of their centers. For structure **2**, the distance between aromatic rings in the nearest neighbouring ligand moieties measures ~ 6 Å, and is edge-to-edge (Figure 1) rather than co-facial. This distance is within the range where inter-chromophore π-π interactions can be substantial[3a], however, the ring centroids are observed to be significantly offset among closest neighbouring ligands, and any inter-ligand interactions are therefore considered to be of an intermediate non-cofacial nature. This is different from the arrangement of **L** in powdered H_2**L**, in which the ligand assumes a herringbone packing arrangement that is quite conducive to significant co-facial arrangement and inter-chromophore π-π interactions. The Stokes shift for **2** was therefore expected and found to be smaller than observed in H_2**L**.

Of note also, is that peaks in the photoemission spectrum for **2** (Figure 4a) lies between those of the two reference substances; i.e., red shifted relative to that of the free ligand (from Na_2**L** in solution, ESI Figure S8), and blue shifted relative to that of powdered H_2**L** (Figure 4b). The red shift is attributed to the presence of intermediate inter-ligand interactions of a non-cofacial nature in the MOF structure compare to the absence of such interactions among the free ligand units in solution. The blue shift observed for **2** relative to powdered H_2**L**, is attributed to the larger separation of the ligands in **2**, and hence a corresponding reduction in the extent of any inter-ligand interactions among the ligand units.[40] This is quite similar to observations reported for Zn stilbene MOFs.[6,7] Another possibility is that the ligand is rigidified in the MOF structure, hence *trans-cis* isomerization is postulated to be suppressed and non-radiative energy loss that would be associated with this geometric change is reduced compared to the ligand in the powdered form. This is also similarly observed in Zn-stilbene MOFs[6,7] and other structures with locked stilbene moieties.[41,42]

Luminescence spectral features from the lanthanide ions were not detected in the visible region (for Tm^{3+}) and was not measured in the near infrared region (for $Tm^{3+}$and Er^{3+}) which is beyond the range of our standard fluorimeter. It is speculated however that photoemissions of these metals ions from direct excitation would be weak or non existent due to their low molar absorption coefficient (typically lower that 10 L mol^{-1} cm^{-1}). Further, *trans*-stilbenedicarboxylate, like most organic ligands, are poor sensitizers of these lanthanide ions, for two main reasons; (i) the low molar absorption coefficients of these metal ions, and (ii)

View Article Online
DOI: 10.1039/C6DT03755K

the very small energy gaps between the first excited state and fundamental level of the metal ions are easily matched by C-H, C=C and O-H vibrations of the ligand, which provide suitable non-radiative channels.[43,44] We speculate therefore that these lanthanide metal ions have no effect on the photoluminencence and radioluminescence behavior of the structures **1** and **2.**

The local environment of the stilbenoid units in the crystals was further probed by time resolved photolumenescence measurements. Emission decay curves for **2** is presented along with H_2**L** in Figure 5. The decay curves were fitted by a biexponential function that corresponds to two different emissive rates and the associated photoluminescence decay lifetimes (ESI Table S16).

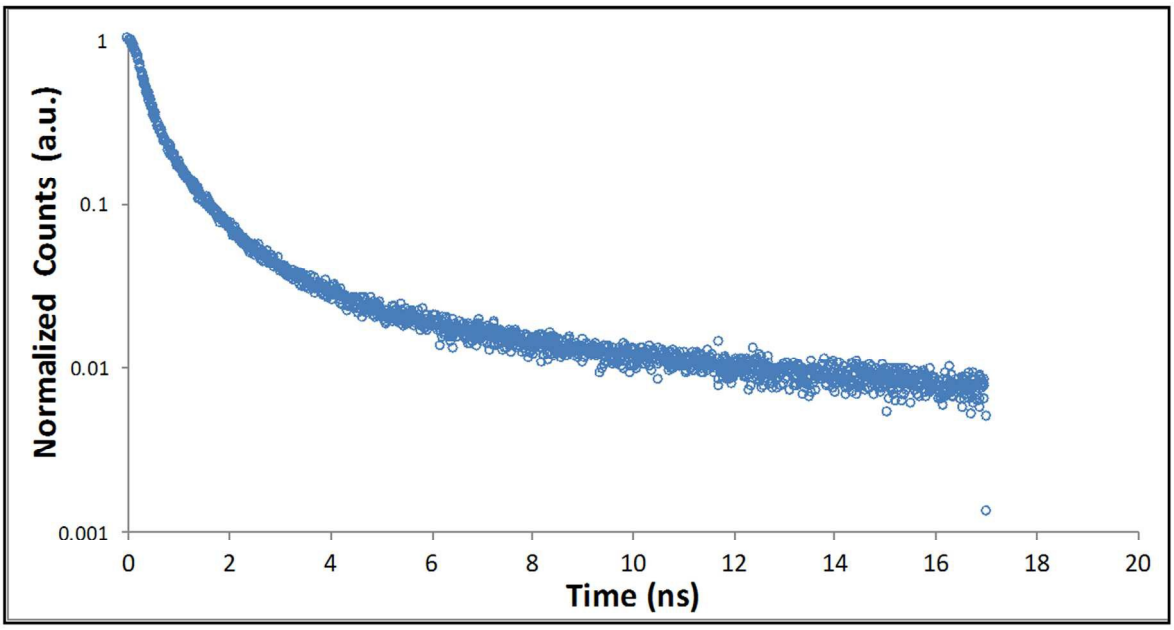

5(a)

View Article Online
DOI: 10.1039/C6DT03755K

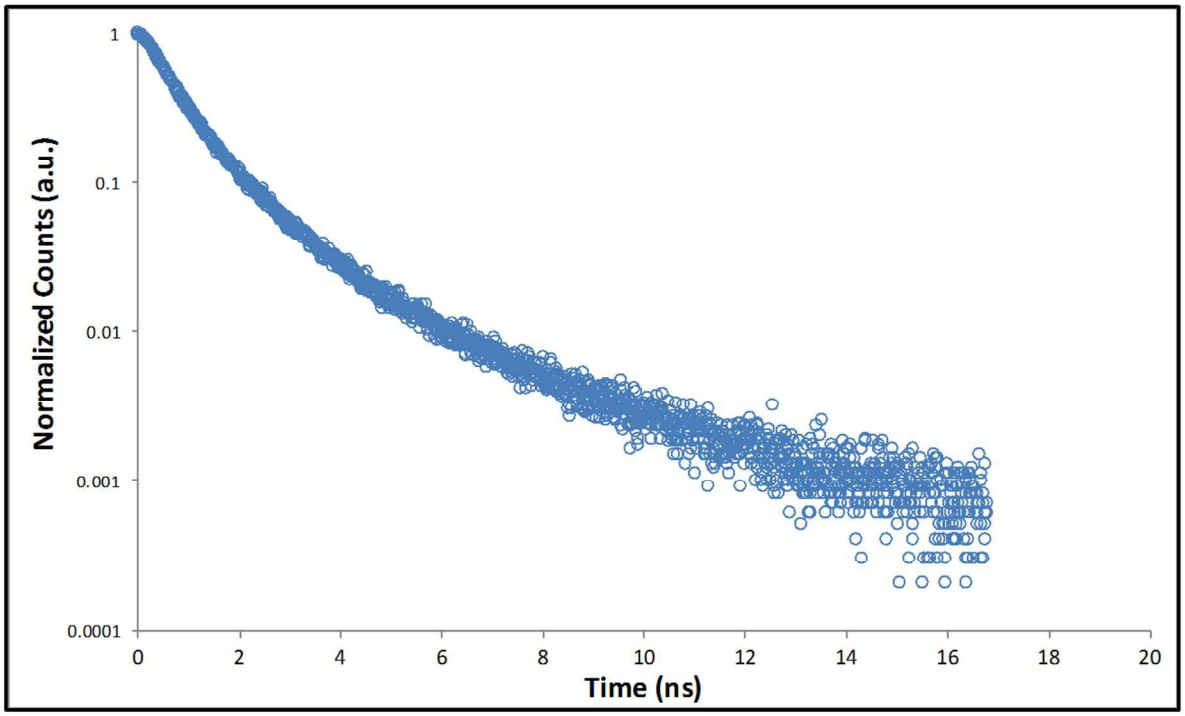

5(b)

Figure 5. Time-resolved emission decay curves of (a) **2** (excited at 440 nm) and (b) H_2**L** (excited at 460 nm).

Among the two emisive rates, the short-lived fast component with lifetime, τ_1, is attributed to emission from monomer stillbenoid units, whereas, a longer-lived component with lifetime τ_2, is attributed to emission from stillbenoid moieties that are involved in coupling interactions, as similarly observed for stilbene dimers.[45] For **2**, τ_1 with a value of 0.4 ns is also observed to be the major component of the lifetime decay. This is within the range observed for Zn (0.2 ns) and other transition metal-stilbenoid based MOFs[7,6], though lower than the value of 0.76 ns we observed for H_2**L** powder. Further, the higher percentage contribution of τ_1 in **2** (α_1 = 89 %) in comparison to that of H_2**L** powder (α_1 = 74 %) is postulated to be attributed to larger predominance of isolated weakly or non-interacting monomeric stilbenoid units in the structure of **2** compared to the H_2**L**. The radiative lifetime (τ) of *trans*-stilbene in solution at room temperature can be reduced to below < 0.1 ns due to *trans-cis* isomerization.[46] Thus the larger value for τ_1 observed for **2** compared to the reported value for *trans*-stilbene in solution, is also consistent with emission from isolated monomeric stilbenoid units that are locked in fixed and

View Article Online
DOI: 10.1039/C6DT03755K

semi-regid configuration within the MOF structure, as their *trans–cis* isomerization activity is suppressed.

Structure **2** shows a second component lifetime, τ_2, that is similar to that observed for H_2**L** powder, suggesting the presence of interchromophore interactions within this large pore structure. However, the lower percentage (α_1 = 11 %) of τ_2 contribution in **2** compared to H_2**L** powder (α_2 = 32 %) is attributed to less through-space interchromophore interactions among the stilbene units, hence a reduction in the extent of the associated non-radiative relaxation pathways in **2**. The photoluminescence behaviour of **2** is consistent with that found by Bauer et al in Zn-stilbene MOFs[6] and by Bazan and coworkers for paracycophane-based stilbene dimers.[47]

Radioluminescence

Unlike photoluminescence, which involves electronic transitions between non-ionized excited states and ground states, radioluminesence (scintillation) is the emission of radiation after a material absorbs radiation with energy generally ≥ 10 eV that leads to π-electron ionization (Iπ).[48] The ionization is followed by ion recombination (the recombining of secondary electrons with their parent electrons) that populates available singlet S, and triplet T, states, and further non-radiative thermal deactivation to the lowest vibrational level of the first excited state S_1 before relaxation to lower electronic levels with an accompanying emission of radiation.[49] Ionization can lead to significant changes in the electronic and molecular structure of material. In this work, two types ionizing radiation were investigated. One was a high energy (2.5 MeV) proton beam from an ion microprobe, as this is known to simulate the production of recoil protons by elastic scattering of fast neutrons within an organic scintillator.[1a] Proton ion beam induced luminescence (IBIL) spectroscopy was therefore used to assess the radioluminescence spectral profile of structures **2** and H_2**L**. For the second, γ radiation with time correlated single photon counting (TCSPC) was used to investigate radioluminescence decay behavior and determine lifetimes.

IBIL: IBIL spectroscopy was used to probe the radio-luminescence characteristics of **2** and H_2**L** under a 2.5 MeV ionizing proton beam at a current density of 12000 nA/cm^2. The IBIL emission profiles are presented along with the corresponding photoluminescence spectra for **2** and H_2**L** in Figures 4a and 4b. A broad featureless emission peak is observed in the IBIL spectrum of both **2** and H_2**L** with λ_{max} visible around 450 and 475 nm, respectively. The

View Article Online
DOI: 10.1039/C6DT03755K

existence of the IBIL spectrum validates that **L**, as a component of the MOF structure, remains radioluminescent. The similarity in the spectral profile of **2** compared to that of H_2**L** shows that the radioluminescence from **2** is a product of the MOF crystal only, and not from any impurities from synthesis or radiation damage.

According to the proposed mechanism of radioluminescence in organic scintillators, triplet excitons that are created by the ionizing radiation, combine to form additional singlets (triplet - triplet annihilation, TA). These singlets then follow similar relaxation pathways as the original singlets and also similar to those in photoluminescence, but with delayed timing. The photoluminescence and radioluminescence emission spectra should therefore overlap.[50] For **2** however**,** a red shift of about 70 nm between the photoluminescence λ_{max} and the IBIL λ_{max} was observed. This is close to the red shift value of about 80 nm that was observed for H_2**L**. It suggests that the relaxation pathway described above was not strictly observed, and that small changes may have occurred in both structures on exposure to the ionizing radiation. Such changes could possibly be a distortion of the chromophore environment, resulting in a shortening of inter-ligand distances and an increase in inter-chromophore interactions, as was similarly observed for Zn-stilbene based MOF.[1] Partial rotation activity around the C=C bond of the **L** in the structures on exposure to the radiation is also a possibility. The IBIL spectrum of **2** was otherwise, comparable to its photoluminescence spectra, indicative of minimal structural damage upon exposure to the ionizing proton beam. It is notable also, that as a result of the significant Stokes shift there was only a relatively small excitation-emission spectral overlap and this is considered to be favorable for the use of the material as a scintillator, in that self-absorption can be minimized by the presence of this shift.[1c]

The Stokes shift between the excitation and IBIL spectra of **2** is less than the 84 nm observed in its open and interpenetrating 3-D Zn stilbene MOF counterpart which contains pores of much smaller dimensions.[1a] This suggests comparatively less adjustment and inter-chromophore interactions in the structure of **2** on exposure to ionizing radiation. The IBIL spectra were also compared with those reported for other open framework MOFs with rigid radioluminescent linkers and with pore dimensions smaller than structure **2**, namely, Zn-IRMOF-10 (containing biphenyldicarboxylate, BPDC), IRMOF-8 (containing 2,6-naphthalenedicarboxylate, NDC), Zn-DUT-6 (containing NDC/benzene 1,3,5-tribenzoate-BTB), Zn-IRMOF-8 (containing NDC), Zn-NOTT-103 (containing

View Article Online
DOI: 10.1039/C6DT03755K

5,5'-(naphthalene-2,6-diyl)diisophthalate, DPNTC) and Zn-PCN-14 (5,5'–(anthracene-9,10-diyl)diidophthalate, DPATC).[1b] Stokes shifts ranging from 11 nm (DUT-6) to 65 nm (IRMOF-8) were observed, which is comparable to that for structure **2.** However, significant differences in their IBIL spectral features in comparison to their photoluminescence spectra indicate structural changes.

Radioluminescence lifetime: Radioluminescence lifetimes were also investigated for **2** and H_2**L**. The samples were irradiated with γ radiation from a ^{137}Cs source. The time resolved radioluminescence logarithmic - scaled curves are plotted in Figure 6. Exponential and non - exponential time components were observed in the decay curves for **2** and H_2**L**. The exponential component is attributed to prompt scintillation, which has lifetime, ($\tau_{s\ prompt}$), and is expected to be equivalent to the photoluminescent lifetime, (τ_F). The longer non-exponential component is ascribed to delayed scintillation ($\tau_{s\ delayed}$), that is associated with triplet-triplet annihilation, and is not observed in photoluminescence.[47] Structure **2** exhibit a $\tau_{s\ prompt}$ value of 1.2 ns which, is within an order of magnitude of the τ_F value of 0.4 ns (ESI Table S16). The $\tau_{s\ prompt}$ value is lower than the 2.0 ns observed for H_2**L**. However, the higher percentage of prompt scintillation (89 %) for **2** compared to that of H_2**L** (68 %) is consistent with the presence of separated and rigidified stilbenoid units within the MOF structure. By comparison, reported time resolved radioluminescence decay data shows that Zn-IRMOF-8 (NDC), Zn-NOTT-103 and Zn-DUT-6 exhibit fast $\tau_{s\ prompt}$ ranging from 8-15 ns and 3 ns for Zn-PCN-14, which are consistent with the isolation of the linkers in the structures, similar to the ligands in dilute solution.[1c] Structure **2** therefore shows a fast component lifetime than is shorter than these MOF structures but higher than the free stilbene ligand in dilute solution.

Of note also is that the delayed scintillation feature is present in **2** with a $\tau_{s\ delayed}$ value of 10 ns, and likewise for H_2**L**. The delayed scintillation which is ascribed to the TA event, is considered an important feature that can be exploited for radiation detection applications to discriminate among radiation from subatomic particles. The technique removes signals from background γ-rays that will occur in organic scintillators used for fast neutrons detection. The delayed luminescence is known to depend on the rate of TA and the lifetime of the triplet excited state, and therefore minimization of other non- radiative deactivation pathway(s) are necessary to increase the relative amount of TA events relative to prompt emission. Though the percentage

View Article Online
DOI: 10.1039/C6DT03755K

delayed scintillation was not quantified, we are postulating, based on the radioluminescence behavior observed for **2**, that spatially separating and rigidifying the stilbenoid units in the MOF structure can lead to enhancement in the amount of delayed luminescence from the ligand, as non-radiative deactivation pathways are minimized and triplet to singlet conversions are facilitated.

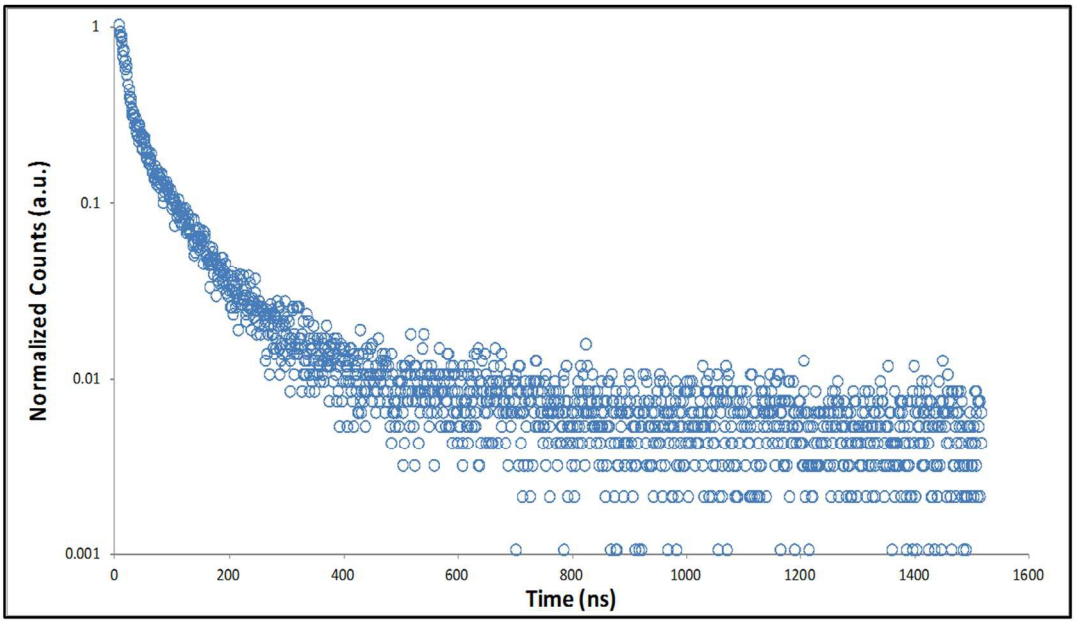

(a)

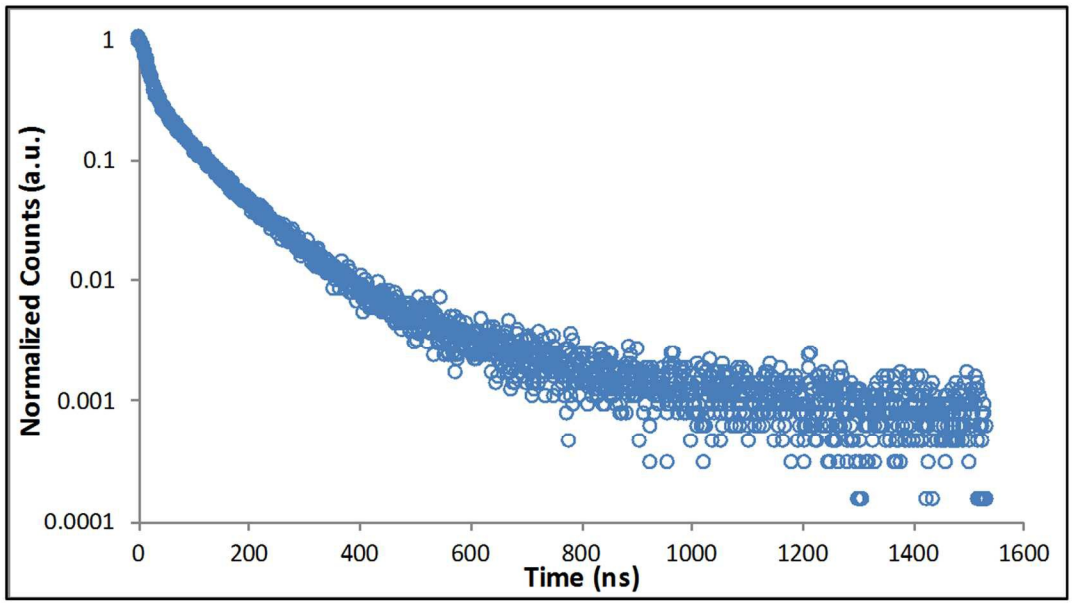

(b)

Figure 6. Time-resolved radioluminescence decay curves for (a) **2** and (b) H_2**L**.

View Article Online
DOI: 10.1039/C6DT03755K

Conclusion

Two isostructural non-interpenetrating 3-D MOFs with ultra large pores are synthesized from the combination of trans- stilbenedicarboxylate and lanthanide metals ions (Tm^{3+} and Er^{3+}). The rigidification of the ligand limits its ability to undergo *trans-cis* isomerization. The isolation of the stilbene units and the absence of interpenetration in this large pore, low density structure limit the ligand's ability to participate in co-facial π-π interactions, thus minimizing any associated non-radiative relaxation pathways. Consequently, the structure exhibits ligand-based photoluminescence with increased lifetime compared to the free stilbene molecules, and also exhibit scintillation behavior which is comprised of both prompt and delayed radioluminescence features.

Acknowledgements

This work was supported by United States National Science Foundation Grants Nos. HRD-0630456, HRD-1305041, and National Nuclear Security Administration Grant No. NA0000979 and Department of Energy Grant No. DE-FE0022952. We thank Dr. Mark Allendorf and Dr. John Perry IV, currently and formerly of Sandia National Laboratories, Livermore, CA, respectively, for their assistance on and insights into the synthesis of MOFs.

Electronic supplementary information (ESI) available: TGA curves, FTIR spectra, PXRD patterns, and the lists of bond lengths, bond angles and other structural details are provided as ESI. Crystallographic data for the structural analysis have been deposited with the Cambridge Crystallographic Data Center as CCDC no. 1501482 and 1501481 for **1** and **2** respectively.

References

1 (a) F. P. Doty, C. A. Bauer, A. J. Skulan, P. G. Grant, and M. D. Allendorf, *Adv. Mater.* 2009, **21**, 95-101. (b) P. L. Feng, J. V. Branson, K. Hatter, G. Vizkelethy, M. Allendorf and F. P. Doty, *Nucl. Inst. Method. Phys. Res*. A 2011, **652**, 295-298. (c) J. J. Perry IV, P. L. Feng, S. T. Meek, K. Leong, F. P. Doty and M. D. Allendorf, *J. Mater. Chem.,* 2012, **22**, 10235-10248.

2 (a) J-. C. G. Bünzli, S. Comby, A-. S. Chauvin, and C. D. B. Vandevyver, *J. Rare Earths,* 2007, **25**, 257-274. (b) G. R. Choppin and D. R. Peterman, *Coord. Chem. Rev.* 1998, **174**,

View Article Online
DOI: 10.1039/C6DT03755K

283-299. (c) F. Gándara, A. García-Cortés, C. Cascales, B. Gómez-Lor, E. Gutiérrez-Puebla, M. Iglesias, A. Monge and N. Snejko, *Inorg. Chem*. 2007, **46**, 3475-3484. (d) W. J. Rieter, K. M. L. Taylor, H. An and W. Lin, *J. Am. Chem. Soc*. 2006, **128**, 9024-9025. (e) R. F. D'Vries, S. Alvarez-Garcia, N. Snejko, L. E. Bausá, E. Gutierrez-Puebla, A. de Andres and M. A. Monge, *J. Mater. Chem. C,* 2013, **1**, 6316 – 6324. (f) B. V. Harbuzaru, A. Corma, F. Rey, P. Atienzar, J. L. Jordá, H. García, D. Ananias, L. D. Carlos and J. Rocha, *Angew. Chem., Int. Ed*. 2008, **47**, 1080 - 1083. (g) A. H. Chughtai, N. Ahmad, H. A. Younus, A. Hussein, Laypkov and F. Verpoort, *Chem. Soc. Rev.* 2015,44, **19**, 6804-6849.

3 (a) J. Cornil, D. A. dos Santos, X. Crispin, R. Silbey and J. L. Bredas, *J. Am. Chem. Soc*., 1998, **120**, 1289-1299. (b) F. Cacialli, B. S. Chauh, J. S. Kim, D. A. dos Santos, R. H. Friend, S. C. Moratti, A. B. Holmes and J. L. Bredas, *Synth Met*. 1999, **102**, 924-925.

4 J. Saltiel, *J. Am Chem. Soc*., 1967, **31**, 1399-1420.

5 A. Simeonov, M. Matsuishita, E. A. Juban, E. H. Thompson, J. Z. Hoffman, A. E. Beuscher, M. J. Taylor, P. Wirsching, W. Rettig, J. K. McCusker, R. C. Stevens, D. P. Millar, P. G. Schultz, R. A. Lerner and K. D. Janda, *Science*, 2000, **290**, 307-313.

6 C. A. Bauer, T.V. Timofeeva, T.B. Settersten, B. D. Patterson, V.H. Liu, B. A. Simmons and M. A. Allendorf, *J. Am. Chem. Soc*. 2007, **129**, 7136-7144.

7 C. A. Bauer, S. C. Jones, T. L. Kinnibrugh, P. Tongwa, R. A. Farrell, A. Vakil, T. Timofeeva, V. Khrustalev and M. Allendorf, *Dalton Trans.* 2014**, 43***,* 2925-2935.

8 (a) J. Luo, H. Xu, Y. Liu, Y. Zhao, L. L. Daemen, C. Brown, T. V. Timofeeva, S. Ma and H-. C. Zhou, *J. Am. Chem. Soc.* 2008, **130**, 9626-9627. (b) S. Q. Ma, X. S. Wang, D. Q. Yuan, and H-. C. Zhou, *Angew. Chem., Int. Ed.* 2008, **47**, 4130-4133. (c) T. Devic, C. Serre, N. Audebrand, J. Marrot and G. Férey, *J. Am. Chem. Soc*. 2005, **127**, 12788. (d) Z. J. Lin, Z. Yang, T. F. Liu, Y. B. Huang and R. Cao, *Inorg. Chem*. 2012, **51**, 1813-1820. (e) K. A. White, D. A. Chengelis, K. A. Gogick, J. Stehman, N. L. Rosi and S. Petoud, *J. Am. Chem. Soc.* 2009, **131**, 18069-18071.

9 X. L. Wang, C. Qin, E. B. Wang and L. Xu, *Cryst. Growth Des*., 2006, **6**, 2061-2065.

10 K. L. Huang, Y. T. Hei and M. Huang, *J. Coor. Chem*. 2008, **61**, 2735-2742

11 J. Yang, J. F. Ma, S. R. Batten and Z. M. Su. *Chem. Commun*, 2008, 2233-2235.

12 H. Y. Wang, S. Gao, L. H. Huo, S. W. Ng and J. G. Zhao, *Cryst. Growth. Des*., 2008, **8**, 665-670.

13 Y. Ma, A. L. Cheng, J. Y. Zhang, Q. Yue and E. Q. Zhao, *Cryst. Growth. Des*., 2009, **9**, 867-876.

View Article Online
DOI: 10.1039/C6DT03755K

14 D. H. Lee and G. Park, *Acta. Crystallogr., Sect.E.* 2008, **64**, M861.

15 G. Park, H. Kim, G. H. Lee, S. K. Park and K. Kim, *Bull. Korean Chem. Soc*., 2006, **27**, 443.

16 J. Yang, J. F. Ma, Y. Y. Liu and S. R. Batten, *CrystEngComm,* 2009, **11**, 151-159.

17 L. Zhang, Y. L. Yao, Y. X. Che and J. M. Zheng, *Cryst. Growth. Des*. 2010, **10**, 528-533.

18 J. Liu and Y. Wang, *J. Chem. Crystallography*. 2011, **41***,* 1940-1944.

19 H-. Y. Wang, S. Gao, J-. G., Zhao and S. W. Ng, *Acta. Crystallogr., Sect. E:* 2006, **62**, M3127.

20 X. L. Wang, Y. Q. Chen, Q. Gao, H. Y. Lin, G. C. Liu, J. X. Zhang and A. X. Tian, *Cryst. Growth Des*., 2010, **10**, 2174-2184.

21 X. L. Wang, Z. C. Guo, G. C. liu, Y. Qu, S. Yang, H. Y. Lin and J. W. Zhang, *CrystEngCommun*., 2013, **15**, 551-559.

22 A. L. Cheng, N. Liu, Y. F. Yue, Y.W. Jiang, E. Q. Gao, C. H. Yan and M. Y. He, *Chem. Commun*., 2007, 407-409.

23 C. A. Bauer, T.V. Timofeeva, T. B. Settersten, B. D. Patterson, V. H. Liu, B .A. Simmons and M. A. Allendorf, *J. Am. Chem. Soc*., 2007, **129**, 7136-7144.

24 A. L. Cheng, Y. Ma, J. Y., Zhang and E. Q. Gao, *Dalton Trans.*, 2008,1993-2004.

25 K. L. Huang, X. Liu and G. M. Liang, *Inorg. Chim. Acta*, 2009, **362**, 1565-1570.

26 A. L. Cheng, Y. Ma, Q. A. Sun and E. Q. Gao, *CrystEngComm.,* 2011*,* **13***, 2721-2726.*

27. A. Naeem, V. P. Ting, U. Hintermair, M. Tian, R. Telford, S. Halim, H. Nowell, M. Hołyńska, S. J. Teat, and I. J. Scowen, *Chem. Commun.*, 2016, **52**, 7826-7829.

28 Z. Deng, L. Huo, H. Wang, S. Gao and H. Zhao, *CrystEngComm.* 2010, **12***,* 1526-1535.

29 Y. Li and D. Song, *Cryst. Eng. Comm.* 2011, **13***,* 1821-1830.

30 *SAINT-Plus* V8.34A, 2013, Bruker AXS Inc., Madison, Wisconsin, USA.

31 *APEX2*, Version 2014.11; Bruker AXS Inc., Madison, Wisconsin, USA.

32 L. Palatinus and G. Chapuis. *J. Appl. Cryst.* 2007, **40**, 786-790.

View Article Online
DOI: 10.1039/C6DT03755K

33 O. V. Dolomanov, L. J. Bourhis, R. J. Gildea, J. A. K. Howard and H. Puschmann, *J. Appl. Cryst.* 2009, **42**, 339–341.

34 A. L. Spek, *Acta Cryst.* C., 2015, 71, **1** , 9-18.

35 G. M. Sheldrick, *Acta Cryst.* 2008, A**64**, 112–122.

36 L. J. Barbour, *J. Appl. Cryst*. 1999, **32**, 353-354.

37 J. Gierschner, H. G. Mack, D. Oelkrug, I. Waldner and H. Rau, *J. Phys. Chem. A* 2004, **108,** 257-263.

38 M. Gudipati, *J. Phys. Chem.* 1993, **97***,* 8602-8607.

39 M. Oelgemoller, B. Brem, R. Frank, S. Schneider, D. Lenoir, N. Hertkorn, Y. Origane, P. Lemmen, J. Lex and Y. Inoue, *J. Chem. Soc., Perkin Trans.* 2002, **2,** 1760-1771.

40 Z-. F. Chen, R-. G. Xiong, J. Zhang, X. T. Chen, Z-. L. Xue and X-. Z. You, *Inorg. Chem.* 2001, **40**, 4075-4077.

41 J. Saltiel, *J. Am. Chem. Soc*., 1967, **89**, 1036-1037.

42 A. Simeonev, M. Matsushita, E. A. Juban, E. H. Z Thompson, T. Z. Hoffman, A. E. Beuscher, J. M. Taylor, P. Wirsching, W. Rettig, J. K McCusker, R. C. Stevens, D. P. Millar, P. G. Schultz, R. A. Lerner and K. D. Janda, *Science*, 2000, **290**, 307-313.

43 J. Rocha, L. D. Carlos, F. A. Almeida Paz and D. Ananias, *Chem. Soc. Rev*., 2011, **40**, 926-940.

44 M. D. Allendorf, C. A. Bauer, R. K. Bhakta and R. J. T. Houk, *Chem. Soc. Rev*., 2009, **38**, 1330-1352.

45 G. C. Bazan, W. J. Oldham, Jr., R. J. Lachiotte, S. Tretiak, V. Chernyak and S. Mukamel, *J. Am. Chem. Soc.,* 1998, **120,** 9188.

46 D. H. Waldeck, *Chem. Rev*., 1991, **91**, 415-436.

47 G. C. Bazan, W. J. Oldman, R. J. Lachiotte, S. Tretiak, V. Chernyak and S. Mukamel, *J. Am. Chem. Soc*., 1998, **120**, 9188-9204.

48 G. F. Knoll, *Radiation Detection and Measurements*, John Riley & Sons, New York, 1989.

49 J. B. Birks, *The Theory and Practice of Scintillation Counting*, Pargamon, Oxford, 1964.

50 T. A. King, R. Voltz, *Proc. R. Soc. London, Ser. A*. 1966, **269** (1418), 424-439.

View Article Online
DOI: 10.1039/C6DT03755K

View Article Online
DOI: 10.1039/C6DT03755K

Graphical abstract

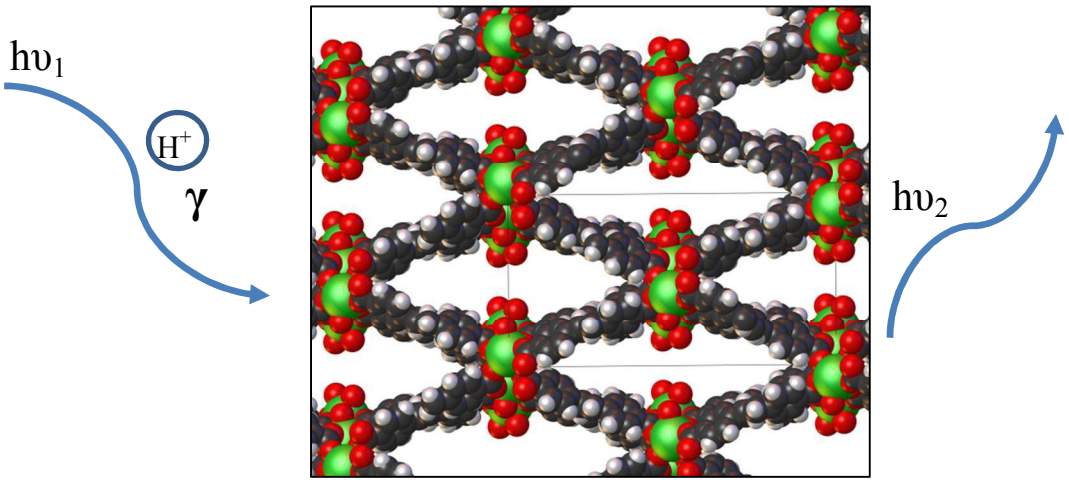

Mesoporous non-interpenetrating stilbene-based lanthanide metal organic framework exhibits photo and radioluminescence behavior.